Journal of Medical Systems (2019) 43: 309
https://doi.org/10.1007/s10916-019-1439-6

IMAGE & SIGNAL PROCESSING

Hip-Joint CT Image Segmentation Based on Hidden Markov Model with Gauss Regression Constraints

Haiyang Liu[1] · Guochao Dai[2] · Fushun Pu[3]

Received: 13 June 2019 / Accepted: 20 August 2019 / Published online: 24 August 2019

Abstract
Hip-joint CT images have low organizational contrast, irregular shape of boundaries and image noises. Traditional segmentation algorithms often require manual intervention or introduction of some prior information, which results in low efficiency and is unable to meet clinical needs. In order to overcome the sensitivity of classical fuzzy clustering image segmentation algorithm to image noise, this paper proposes a fuzzy clustering image segmentation algorithm combining Gaussian regression model (GRM) and hidden Markov random field (HMRF). The algorithm uses the prior information to regularize the objective function of the fuzzy C-means, and then improves it with KL information. The HMRF model establishes the neighborhood relationship of the label field by prior probability, while CRM model establishes the neighborhood relationship of feature field on the basis of the consistency between the central pixel label and its neighborhood pixel label. The experimental results show that the proposed algorithm has high segmentation accuracy.

Keywords Hip-joint segmentation · Low contrast · CT image · Hidden Markov model · Gaussian regression model · Neighborhood relationship

Introduction

Computer-aided diagnosis (CAD) is a hot research topic in the field of medical image processing in recent years [1]. It is a key technology to alleviate the pressure of doctors and improve the utilization rate of medical resources [2]. At present, computer diagnosis can not completely replace doctor diagnosis. Therefore, using computer technology to assist doctors in diagnosis is an effective way to improve the efficiency of diagnosis and treatment. With the development of medical imaging and information processing, the CAD technology has made great progress, so it has been highly valued by medicine experts at home and abroad [3, 4].

At present, the research on computer-aided diagnosis is mainly divided into the following aspects: (1) image denoising and reconstruction is to obtain clear medical image [5]; (2) medical diagnosis fuzzy expert system technology can carry out preliminary diagnosis for common diseases [6]; (3)Three-dimensional reconstruction of medical images is used to assist the diagnosis of bone dislocation [7, 8]; (4) automatic segmentation of medical images can extract lesions, quantify image information, and so on [9]. In all applications, automatic image segmentation is an important technology for medical image diagnosis. For various medical images, such as cells, bones, tumors, etc., different segmentation methods have their own advantages, and scholars need to carefully choose [10]. Literature [5] proposed a lung nodule recognition method based on multi-view deep belief network, which can effectively segment lesions and reduce false positive diagnosis. Literature [11] used a mixture-based priori algorithm to segment the CT series frame by frame and reconstruct then as three-dimensional structure so as to show the positional relationship between the medullary mortar and the femur [11]. Medical image registration refers to the alignment of a medical image with a corresponding point on another image. Xia

This article is part of the Topical Collection on *Image & Signal Processing*

✉ Fushun Pu
hhzfskmri@126.com

[1] Department of Radiology, Shangluo Central Hospital, Shangluo 726000, Shaanxi, China

[2] Image Center of the First People's Hospital of Kashgar, Kashgar, Xinjiang 844000, China

[3] Southern Central Hospital of Yunnan Province (The First People's Hospital of Honghe State), Mengzi 661199, Yunnan, China

et al. used feature matching and geometric priori to register rigid body images with non-rigid images, and the matching success rate is high [12]. Chandra et al. used biophysical models for registration and segmentation of cardiac images, but relied heavily on offline, complex training sets [13]. Kim et al. used a layered algorithm combined with Hough transform to segment and identify the pelvis, which requires a fairly large training set and has limitations in image processing of various poses [14]. Luis-Garcia et.al [9] use the bone density grayscale and image shape features in CT images to design an auxiliary diagnostic algorithm for determining the presence of osteoporosis in the thoracolumbar spine center, which has certain practical significance.

Hip joint is an important joint connecting pelvic bone and thigh bone, as shown in Fig.1. It bears weight and controls the movement of lower limbs [8]. It is prone to abrasion and deformation, which affects people's normal life. Artificial joint replacement can restore joint activity by replacing injured joint surface with prosthesis. In order to make the artificial joint fit the biological and physical characteristics of the patient's own joint as much as possible, it is necessary to measure the three-dimensional characteristics of the healthy joint. The surface data of the hip joint (i.e. the outline data) is the basis of the three-dimensional feature measurement, and directly affects the accuracy of the measurement results. Therefore, extracting joint surface data is the basis and basis for making artificial joints suitable for patients.

CT sequence images of the hip joint provide a new way to understand the hip joint, and they have significant features different from other sequence images, such as low contrast of images, close connection between acetabulum and femoral head, etc. So there are many corresponding segmentation algorithms which have been proposed to solve these questions. Literature [14] used the Snake model to extract the external contour of the hip joint, and an initial contour setting method based on the central radiation algorithm is proposed to extract the quasi-circular part. The algorithm is feasible, but the noise resistance of the method is poor. Literature [15] adopts the adaptive Graph Cuts algorithm to locate and segment the femoral head accurately which can obtain better extraction results, but the algorithm has high complexity and low efficiency. According to the similarity of CT sequence images, literature [16] proposes a recognition model based on the front frame contour along the normal direction as a priori, which can recognize the image with uniform skeletal changes better, but the image recognition effect of local skeletal mutations is not good.

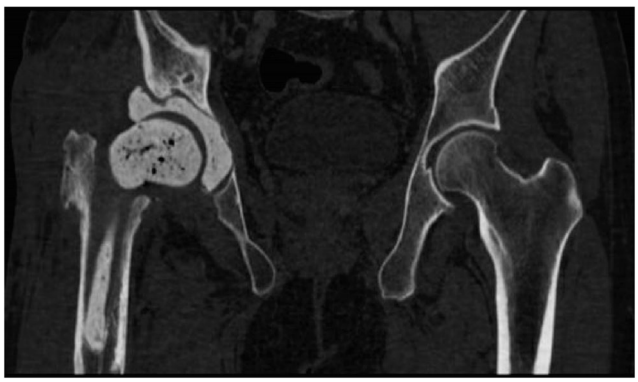

Fig. 1 Hip joint for a patient in CT image

In order to overcome the sensitivity of classical fuzzy clustering image segmentation algorithm to image noise, this paper proposes a fuzzy clustering image segmentation algorithm combining Gaussian regression model (GRM) and hidden Markov random field (HMRF). The algorithm uses the information to regularize the objective function of the fuzzy C-means, and then improves it with KL information, and applies the HMRF and CRM models to the objective function. The HMRF model establishes the neighborhood relationship of the label field by prior probability, while CRM model establishes the neighborhood relationship of feature field on the basis of the consistency between the central pixel label and its neighborhood pixel label. The proposed algorithm and other classical algorithms are used to segment the CT hip-joint image, and the accuracy of the segmentation results is evaluated. The experimental results show that the proposed algorithm has high segmentation accuracy.

Materials and methods

In Non-Fuzzy Segmentation, each pixel can only belong to a certain category, while each pixel can belong to all categories in Fuzzy Segmentation, and the fuzzy membership degree is used to indicate the degree of different categories to which the pixels belong [17]. This method needs to define the non-similarity measurement between pixels and clustering centers, and use the fuzzy membership measurement and non-similarity measurement to establish the objective function, and then achieve image segmentation by minimizing the objective function. In the FCM algorithm, the objective function is defined as:

$$J_{fcm}(U,V) \triangleq \sum_{i=1}^{N}\sum_{j=1}^{o} u_{ij}^{m} d_{ij} \tag{1}$$

where $d_{ij} = \|x_i - \upsilon_j\|^2$ represents the Euclidean distance between pixel x_i and clustering center υ_j, where $x = \{x_i; i = 1, \cdots, N\}$ is the image to be segmented, i is the index of pixels, N is the number of pixels, x_i is the intensity of the ith pixel in the image. $U = |u_{ij}|_{N \times o}$, u_{ij} represents the membership degree of the ith pixel in class j, m is the fuzzy factor, which represents the fuzzy degree of the algorithm; C represents the number of categories. $V = (\upsilon_1, \cdots, \upsilon_j, \cdots, \upsilon_o)$, where υ_j is the clustering center of the $j$the category.

By introducing information entropy and a positive parameter, a new objective function is defined and the EFCM algorithm is proposed. The objective function can be expressed as:

$$J_{efcm}(U,V) \triangleq \sum_{i=1}^{N}\sum_{j=1}^{c} u_{ij}d_{ij} + \lambda \sum_{i=1}^{N}\sum_{j=1}^{c} u_{ij}\ln u_{ij} \tag{2}$$

The second item in Eq. (2) is the stop regularization term, which indicates the fused degree of the segmentation results. Its coefficient is taken as a fuzzy factor to indicate the fuzzy degree of the algorithm.

On the basis of EFCM, KL information and HMRF model are introduced to obtain the HMRF-EFCM algorithm. The objective function can be rewritten as follows:

$$J_{\lambda}(U,\mu,\sigma,\pi) \triangleq \sum_{i=1}^{N}\sum_{j=1}^{o} u_{ij}d_{ij} + \lambda \sum_{i=1}^{N}\sum_{j=1}^{o} u_{ij}\ln\left(\frac{u_{ij}}{\rho_{ij}}\right) \tag{3}$$

where ρ_{ij} is a weight parameter, and the second item in Eq. (3) can also be regarded as a regularization term, indicating the fused degree of the segmentation results. Generally, FCM algorithm can easily segment the edge part of large region clustering to small region clustering. Eq. (3) as the objective function can largely avoid the above problems. However, the HMRF-EFCM algorithm only considers the label field neighbourhood, but does not consider the feature field neighbourhood.

Based on the HMRF-EFCM algorithm, this paper proposes a fuzzy clustering image segmentation algorithm combining GRM and HMRF, which considers both label field neighborhood and feature field neighborhood. Based on the Gauss model, the GRM model introduces neighborhood pixels with the same label as the central pixel to establish the neighborhood relationship of the feature field. Then, the model is used to define the non-similarity measurement d_{ij}.Under given label l_j, observe the negative natural logarithm of probability density function of data x_i.

$$d_{ij}(\theta_j) \triangleq -\ln p(x_i|l_j;\theta_j) \tag{4}$$

where $(l_1, l_2, \cdots, l_j, \cdots, l_N)$ is an implementation of label field $L = (L_1, L_2, \cdots, L_j, \cdots, L_N)$, and $l_j \in \{1, 2, \cdots, c\}$, $\theta_j = (\mu_j, \sigma_j)$ is a parameter vector composed of the mean and variance of the seventh category. Because GRM model is based on the assumption that neighborhood pixels and central pixels have the same label, this assumption may not be valid in practice. In order to solve this problem, when constructing GRM model, only the neighborhood pixels which are consistent with the central pixel label are considered, and the neighborhood pixels which are inconsistent with the central pixel label are not considered. That is to say, when the neighborhood pixel is identical with the central pixel label, its action coefficient is set to 1; when the neighborhood pixel is not identical with the central pixel label, its action coefficient is set to 0. Therefore, the indicator function is defined as:

$$t(l_i, l_{i'}) = \begin{Bmatrix} 1, & l_{i'} = l_i \\ 0, & l_{i'} \neq l_i \end{Bmatrix} \tag{5}$$

where l_i denotes the label of i, i' denotes the neighborhood pixels of i, and $l_{i'}$ denotes the label of i'. The probability density function of GRM model is:

$$p\left(x_i|L_i = j, \theta_j, L_{i'}, i' \in N_i\right) = \frac{1}{\sqrt{2\pi\sigma_j^2}} \cdot \exp\left\{-\frac{\left(x_i - \mu_j\right) + \beta \sum_{i' \in N_i} t\left(L_i, L_{i'}\right)\left(x_{i'} - \mu_j\right)}{2\sigma_j^2}\right\} \tag{6}$$

where $\theta_j = (\mu_j, \sigma_j)$, N_i is the neighborhood set of pixel i, μ_j and σ_j are the mean and variance of class j, β is the parameter to express the intensity of neighborhood action. The larger β is, the greater the intensity of neighborhood action; the smaller β is, the smaller the intensity of neighborhood action. Compared with the traditional Gauss model, GRM model introduces the error effect of neighborhood pixels which are consistent with the central pixel label on the basis of the central pixel error, that is, the second item in Eq. (6). When $\beta = 0$, GRM model has the same effect as Gauss model. When $\beta \neq 0$, the neighborhood pixels consistent with the label of the central pixel will strengthen its role with the central pixel, and the pixels with the same label are easier to belong to the same category. The introduction of neighborhood relationship enhances the interaction between neighborhood pixels and central pixels, making it easier for adjacent pixels to belong to the same category. On the basis of labeling field neighborhood, introducing feature field neighborhood relationship further strengthens the intensity of interaction between neighborhood pixels and central pixels, which is more conducive to eliminating noise and abnormal values and obtain more reliable segmentation results.

p_{ij} in Eq. (3) is the prior probability of HMRF model. In general, neighborhood pixels are more likely to have the same label than non-neighborhood pixels. In order to make the potential energy function smaller and its corresponding prior probability larger, the prior probability is defined as the negative exponent of the sum of potential energy function c, and normalized to make the sum of different categories equal to 1. The prior probability that the pixel ***I*** belongs to class ***j*** is:

$$p_{ij} \triangleq p\left(l_i = j\middle|\hat{l}_{\partial j}; b\right) = \frac{\exp\left(-b \sum_{i' \in N_i} V_{i'}\left(j - l_{i'}\right)\right)}{\sum_{j'=1}^{c} \exp\left(-b \sum_{i' \in N_i} V_{i'}\left(j' - l_{i'}\right)\right)} \tag{7}$$

where $\boldsymbol{b}$ is a parameter to characterize the action intensity of neighborhood labeling. V_c is a potential energy function, which can be defined as:

$$V_{i'}(l_i - l_k) = \begin{Bmatrix} 0, & l_i = l_k \\ 1, & l_i \neq l_k \end{Bmatrix} \tag{8}$$

The prior probability defined by Eq. (7) introduces the neighborhood pixel effect into the labeling field. Because the neighborhood pixel effect enhances the intensity of the interaction between the neighborhood pixel label and the central pixel label in the labeling field, the segmentation precision of the algorithm is improved to a certain extent.

In order to minimize the objective function of Eq. (3), the partial derivative of the objective function to u_{ij} is obtained. And it is equal to 0, and then it can be solved that:

$$u_{ij} = \frac{\rho_{ij}\exp\left(-(1/\lambda)d_{ij}\right)}{\sum_{j'=1}^{c} \rho_{ij'}\exp\left(-(1/\lambda)d_{ij'}\right)} \tag{9}$$

By substituting Eq. (6) into Eq. (4), the expression of d_{ij} can be obtained as follows:

$$d_{ij} = -\ln\left\{\left(\frac{1}{\sqrt{2\pi\sigma_j^2}}\right)\exp\left[-\left(\left(x_i - \mu_j\right) + \beta\sum_{i' \in N_i} t\left(L_i, L_{i'}\right)\left(x_{i'} - \mu_j\right)\right)^2 / \left(2\sigma_j^2\right)\right]\right\} \tag{10}$$

The objective function in Eq. (3) is used to find partial derivatives of μ_j and σ_j, and make them equal to zero. The parameters μ_j and σ_j are:

$$\mu_j = \frac{\sum_{i=1}^{N} u_{ij}\left[x_i + \beta\sum_{i' \in N_i} t\left(L_i, L_{i'}\right)x_{i'}\right]}{\sum_{i=1}^{N} u_{ij}\left[1 + \beta\sum_{i' \in N_i} t\left(L_i, L_{i'}\right)\right]} \tag{11}$$

$$\sigma_j^2 = \frac{\sum_{i=1}^{N} u_{ij}\left[\left(x_i - \mu_j\right) + \beta\sum_{i' \in N_i} t\left(L_i, L_{i'}\right)\left(x_{i'} - \mu_j\right)\right]^2}{\sum_{i=1}^{N} u_{ij}} \tag{12}$$

The main frame of proposed segmentation scheme

Eq. (9)-Eq. (12) show that the neighborhood relationship of feature field not only embodies in the non-similarity measurement, but also affects expectation, variance and membership. The neighborhood relationship of the label field also affects the prior probability and membership degree. It can be seen that the combination of feature field neighborhood and label field neighborhood can greatly improve the precision of image segmentation. In summary, the proposed algorithm can be summarized as follows:

Step 1: set the cyclic indicator k = 0, clustering number c, fuzzy factor λ and iteration stopping condition parameter ε;
Step 2: randomly initialize the membership function $u_{ij}^{(0)}$;
Step 3: calculate the prior probability $\rho_{ij}^{(k)}$ based on Eq. (7) and Eq. (8);
Step 4: estimate the mean and promote the variance $\sigma_j^{(k)}$ by Eq. (11) and Eq. (12);
Step 5: calculate $d_{ij}^{(k)}$ by substituting $\mu_j^{(k)}$ and $\sigma_j^{(k)}$ into Eq. (10)
Step 6: calculate fuzzy membership degree based on Eq. (9);
Step 7: If $\max|U^{(b)} - U^{(b+1)}| < \varepsilon$, stop the loop, otherwise let k = k + 1 and go back to step 3 to continue iterating.

The difference between fuzzy segmentation and non-fuzzy segmentation is that the former uses the fuzzy membership degree to represent the class attributes of the pixels, while the latter makes the pixels clearly belong to a certain object class. In order to get a clear segmentation result, the fuzzy membership matrix $\boldsymbol{U}$ is defuzzification. In this paper, the maximum membership criterion is used to realize the defuzzification:

$$C_i = \arg_j\left\{\max\left\{u_{ij}\right\}\right\}, j = 1, \cdots c; i = 1, \cdots, N \tag{13}$$

where C_i represents the category of pixel i, and $C = \{C_1, C_2, \cdots, C_N\}$ denotes the result of the non-fuzzy segmentation.

Experimental results and analysis

CT data sources

The CT data are all from third-class A hospitals in this paper. In order to facilitate qualitative and quantitative performance analysis, all images are labeled by experts in the industry as a benchmark library for comparison. In the CT data used in this paper, there are two types of CT hip joint images, which is due to the difference between CT images obtained from different angles. From the bottom to the top, the skeletal region of the femoral head has a large change on one side of the femoral head (as shown in Fig. 2 (a). From the top to the bottom, the greater trochanter and the femoral head are two parts of the skeleton at first, and the larger mutation on the one side of the greater trochanter (as shown in Fig. 2 (b)) is found in the combined sections of the greater trochanter and the femoral head.

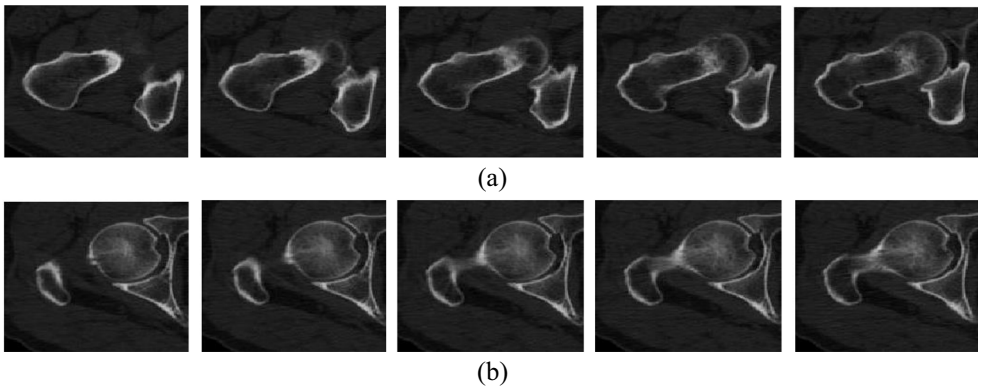

Fig. 2 Partial data sets for different types; (a) From the bottom to the top; (b) From the top to the bottom

Experimental settings

In order to quantitatively evaluate the segmentation effect of the algorithm, this paper uses two common evaluation indicators, namely, Dice similarity coefficient (DSC) and means absolute distance (MAD). DSC denotes the similarity between the contour regions of two images. The larger the value, the better the segmentation effect. MAD measures the average absolute distance between the segmentation result and the real ground truth of artificial segmentation. The smaller the value, the higher the segmentation accuracy. In addition, in order to evaluate the proposed algorithm quantitatively, five representative images are selected for comparison analysis, namely, FCM, FCM_S [18], EnFCM, FGFCM [19], FLICM and HMRF-FCM [20].

Qualitative and quantitative analysis

Figure 3(b)~Fig. 3(f) are the segmentation results of the comparison algorithm, and Fig. 3(g) is the segmentation results of the proposed algorithm. FCM algorithm only considers the influence of the pixels on the segmentation, so it is sensitive to image noise and abnormal value. As shown in Fig. 3 (b), there are a large number of pixels which are segmented in error in FCM algorithm. The neighborhood effect is added to FCM_S algorithm, which improves the segmentation result to a certain extent. As can be seen from Fig. 3(c) and Fig. 3(d), EnFCM and FGFCM cannot effectively segment hip-joint regions, because both of them are accelerated algorithms of FCM algorithm. The segmentation result of FGFCM is slightly better than that of EnFCM, because the introduction of spatial relationship in FGFCM enhances the description performance of the algorithm. FLICM controls the balance between background and image details through an automatically acquired fuzzy coefficient, which improves the adaptability of the algorithm. The fuzzy coefficients obtained in this example are more conducive to hip-joint control, and neglect the protection of object details, resulting in edge blurring. HMRF-FCM introduces HMRF model to establish the neighborhood relationship between label fields, which has good adaptability to noise. But it does not consider the neighborhood relationship of feature fields, which makes it difficult to identify region [21]. The FCM algorithm and its improved algorithm do not consider the spatial distribution of the pixels. In the region where the two distribution curves coincide, the classification of the pixels cannot be effectively distinguished [21]. It can be seen from the results of Fig.3(g) that the proposed algorithm can suppress noise, improve the anti-noise ability and separate homogeneous regions better because it considers both the label field neighborhood and the feature field neighborhood. The experimental results show that the variance in homogeneous region has a great influence on the segmentation results. Because

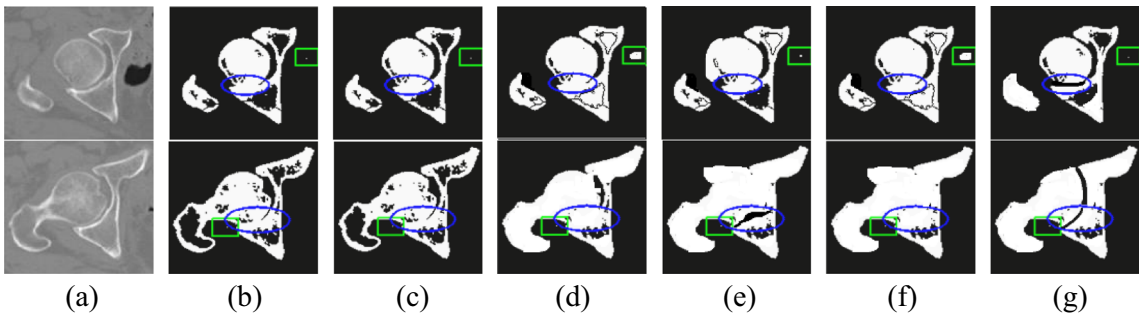

Fig. 3 Segmentation results for different comparison algorithms

Table 1 Comparison of segmentation results for different methods

Methods	FCM	FCM_S	EnFCM	FGFCM	FLICM	HMRF-FCM	Proposed
DSC	0.86	0.88	0.91	0.89	0.90	0.95	0.97
MAD	38.69	29.25	24.92	26.25	25.85	15.21	12.58

of the small variance between the medullary mortar and the femur, all the algorithms can segment the region well. The region tool has the largest variance, so the segmentation effect of the five regions is the worst. However, the proposed algorithm can effectively segment regions with large differences, and the number of erroneous pixels in the segmentation results is less; while there are a large number of erroneous pixels in the segmentation results of other algorithms, which cannot achieve the segmentation of regions with large gray variance [22].

In order to evaluate the precision of the above different segmentation methods, segmentation accuracy mean statistics of different segmentation methods is shown in Table 1. The higher the value of each index, the higher the segmentation precision. Table 1 shows that, except FLICM algorithm, the overall precision of other algorithms is not more than 80%, and the maximum DSC value is 0.71; the overall precision of FLICM algorithm is 96.9%, and the DSC value is 0.96. The overall precision of the proposed algorithm is 99.3%, and the DSC value is 0.99. therefore, our proposed segmentation method in this paper has higher accuracy, lower error rate and better segmentation effect.

Conclusions

Hip-joint CT images have low organizational contrast, irregular shape of boundaries and image noises. Traditional segmentation algorithms often require manual intervention or introduction of some prior information, which results in low efficiency of segmentation and is unable to meet clinical needs. In order to overcome the sensitivity of classical fuzzy clustering image segmentation algorithm to image noise, this paper proposes a fuzzy clustering image segmentation algorithm combining Gaussian regression model (GRM) and hidden Markov random field (HMRF). The experimental results show that the proposed algorithm has high segmentation accuracy.

Compliance with Ethical Standards

Conflict of Interests The authors declare that there is no conflict of interests of this paper. This article does not contain any studies with human participants or animals performed by any of the authors. Informed consent was obtained from all individual participants included in the study.

References

1. Diekhoff, T., Hermann, K.G.A., and Greese, J. et al., Comparison of MRI with radiography for detecting structural lesions of the sacroiliac joint using CT as standard of reference: Results from the SIMACT study[J]. *Ann. Rheum. Dis.* 201639–210640, 2017.
2. Zhang, H., Dong, B., and Liu, B., A reweighted joint spatial-radon domain CT image reconstruction model for metal artifact reduction[J]. *SIAM J. Imag. Sci.* 11(1):707–733, 2018.
3. Tim, V.D.W., Paycha, F., and Klaus, S. et al., SPECT/CT in postoperative painful hip arthroplasty[J]. Seminars in Nuclear Medicine, S0001299818300394, 2018.
4. Tümer Nazl, A. K., Frans, V. et al., Three-dimensional registration of freehand-tracked ultrasound to CT images of the Talocrural joint[J]. *Sensors* 18(7):2375–2389, 2018.
5. Ren, X., Xiang, L., Nie, D. et al., Interleaved 3D-CNNs for joint segmentation of small-volume structures in head and neck CT images[J]. *Med. Phys.* 24(3):65–74, 2018.
6. Liao, H., Mesfin, A., and Luo, J., Joint vertebrae identification and localization in spinal CT images by combining short- and long-range contextual information.[J]. *IEEE Trans. Med. Imag.* 120(99):1–17, 2018.
7. Bottoms, L., and Sinclair, J., Effects of different footwear on distribution of hip-joint contact stress[J]. The Lancet, 389–428, 2017.
8. Kainmueller D, Lamecker H, Zachow S, et al. An articulated statistical shape model for accurate hip joint segmentation[C]// international conference of the IEEE engineering in Medicine & Biology Society. IEEE, 109–203, 2009.
9. Luis-Garcia, R.D., and Alberola-Lopez, C., Parametric 3D hip joint segmentation for the diagnosis of developmental dysplasia.[C]// international conference of the IEEE engineering in Medicine & Biology Society. IEEE, 2087–2099, 2006.
10. Chandra, S. S., Xia, Y., Engstrom, C. et al., Focused shape models for hip joint segmentation in 3D magnetic resonance images[J]. *Med. Image Anal.* 18(3):567–578, 2014.
11. Von, J. U., Overhoff, H. M., and Lazovic, D., 3-D visualization of the newborn's hip joint using ultrasound and automatic image segmentation[J]. *Stud. Health Technol. Inform* 77:1170–1174, 2000.
12. Xia, K., Zhong, X., Zhang, L., and Wang, J., Optimization of diagnosis and treatment of chronic diseases based on association analysis under the background of regional integration. *J. Med. Syst.* 43: 46, 2019. https://doi.org/10.1007/s10916-019-1169-9.
13. Chandra, S., Xia, Y., Engstrom, C. et al., Unilateral hip joint segmentation with shape priors learned from missing data[J]. *Proc. / IEEE Int. Symp. Biomed. Imag. nano macro. IEEE Int. Sym. Biomed. Imag.* 2012:1711–1714.
14. Kim, J. J., Nam, J., and Jang, I. G., Fully automated segmentation of a hip joint using the patient-specific optimal thresholding and watershed algorithm[J]. Comput. Methods Programs Biomed. 154:161, 2018.
15. Sanding, L., Segmentation method for proximal femur in CT images of hip joint[J]. Comput. Eng. Applic. 47(20):171–174, 2011.
16. Xia, K., Gu, X., and Zhang, Y., Oriented grouping-constrained spectral clustering for medical imaging segmentation. *Multimed. Syst.* 6 2019. doi:https://doi.org/10.1007/s00530-019-00626-8.
17. Xia, K., Yin, H., and Zhang, Y.-D., Deep semantic segmentation of kidney and space-occupying lesion area based on SCNN and

ResNet models combined with SIFT-flow algorithm. *J. Med. Syst.* 43(1):2–12, 2019.

18. Zhou, S., Cheng, Y., Wang, Y. et al., Segmentation of the hip joint in CT volumes using adaptive thresholding classification and normal direction correction[J]. *J. Chin. Instit. Eng.* 36(8):1059–1072, 2013.
19. Xia, Y., Chandra, S. S., Engstrom, C. et al., Automatic hip cartilage segmentation from 3D MR images using arc-weighted graph searching[J]. *Phys. Med. Biol.* 59(23):7245–7266, 2014.
20. Wang, J., Cheng, Y., Fu, Y. et al., Segmenting the femoral head and acetabulum in the hip joint automatically using a multi-step Scheme[J]. *IEICE Trans. Inform. Syst.* E95-D(4):1142–1150, 2012.
21. Overhoff, H. M., Jan, U. V., and Lazovic, D., Visualization of a newborn's hip joint using 3D ultrasound and automatic image processing[J]. *Proc. Spie* 3661(4):549–563, 1999.
22. Xia, K., Yin, H., Qian, P., Jiang, Y., and Wang, S., Liver semantic segmentation algorithm based on improved deep adversarial networks in combination of weighted loss function on abdominal CT images. *IEEE Access* 7:96349–96358, 2019.